Mechanism and Machine Theory 210 (2025) 106010

Contents lists available at ScienceDirect

Mechanism and Machine Theory

journal homepage: www.elsevier.com/locate/mechmt

Research paper

Projective synthesis of planar compliant mechanisms

O. Sorgonà [a], O. Giannini [a], M. Verotti [b,*]

[a] Department of Engineering, Niccoló Cusano University of Rome, Via Don Carlo Gnocchi 3, 00166 Rome, Italy
[b] Department of Mechanical, Energy, Management and Transportation Engineering, University of Genova, Via all'Opera Pia 15, 16145 Genoa, Italy

ARTICLE INFO

Keywords:
Compliant mechanisms
Compliant mechanisms synthesis
Flexures
Projective geometry
Parallel compliant mechanisms
Hybrid topologies

ABSTRACT

In this paper, a novel method for the synthesis of planar compliant mechanisms, based on projective geometry, is presented. The *projective synthesis method* exploits the antiprojective polarity in the weighted projective plane, enabling the extension of single-point to single-body relations. The method consists of a top-down procedure that, starting from the load–displacement requirements, defines the elastic suspension as a system of substructures in series and parallel arrangements, according to the prescribed topology. The geometric decomposition intrinsically guarantees positive definiteness of the kinetostatic relations at any level. Multiple solutions to the synthesis problem can be generated. The method has been implemented to the synthesis of compliant mechanisms with open and closed chains, and numerical simulations have been performed to validate the theoretical model.

1. Introduction

In the last years, many investigations focused on the development of analysis and modeling methods for compliant mechanisms, both at the element level [1–5] and at the mechanism level [6–10]. At the same time, due to the requirements imposed by the increasing range of applications, the synthesis problem became a scientific topic of fundamental interest. Generally, the synthesis approaches can focus on the output port of the compliant system or on the whole mechanism.

In the first case, the procedures follow the methods based on the rigid-body kinematics [11–13]. In the single-point synthesis method, the motion of the end-effector is exploited to find the points on the moving plane that satisfy load–displacement requirements [14]. In the geometric invariants synthesis, specific motion paths are obtained considering the high-order kinematics of the system [15].

In the second case, the synthesis procedures work at the mechanism level, defining a compliant structure that meets assigned functional requirements. The methods belonging to this category are briefly described in the following part.

Topology optimization computes the best pattern of material distribution within the design space, by considering cost functions and constraints. A variety of methodologies have been developed [16,17], based on different parametrizations, with truss, beam, bilinear, or quadrilateral elements [18–21]. These methods can lead to effective and innovative designs. However, the obtained configurations could require additional refinements that may compromise the quality of the solution [22]. Also, the design of complex mechanisms poses significant challenges [23].

The rigid-body-replacement method consists of transforming a rigid-body mechanism into a compliant one, by replacing the kinematic pairs with flexure hinges [24,25]. The replacement is performed by resorting to the pseudo-rigid body model, that links the load–deflection characteristics of the two systems. Various pseudo-rigid body models have been proposed in literature, with one

* Corresponding author.
E-mail address: matteo.verotti@unige.it (M. Verotti).

https://doi.org/10.1016/j.mechmachtheory.2025.106010
Received 24 November 2024; Received in revised form 20 January 2025; Accepted 19 March 2025
Available online 8 April 2025

or more degrees of freedom [26–32]. This approach makes available to compliant mechanisms the synthesis tools of the rigid-body kinematics, but the design of the rigid-body mechanism remains an essential prerequisite.

The freedom and constraint topologies approach provides a visual map to find solutions for complex compliant mechanisms [33, 34]. The method, based on a library of vector spaces derived from screw theory and exact-constraint design, has been applied for mechanisms with series and parallel configurations [35–37].

Other methods focused on the requirement of motion decoupling. The constraint and position identification approach introduced the concept of position space for the synthesis of decoupled spatial translational compliant parallel manipulators [38]. The constraint-flow based method was developed for the synthesis of decoupled $XY\theta$ mechanisms [39], whereas decoupling with isotropic property has been considered in Ref. [23].

According to the building block method, the compliant mechanism is defined as a network of compliant blocks characterized by load–displacement relations between their input and output ports [40,41]. A compliant building elements approach, based on a library of compliant elements to be used for generating the required topological designs, has been proposed [42]. Also, the geometry associated to the linear kinetostatics of an elastic suspension has been described through eigentwists and eigenwrenches relations, and used for the concatenation of the elements [43]. In the case of planar compliant systems, the geometric framework can be described by two entities, which are the center of elasticity and two force-compliant axes [44,45]. In this scenario, a building blocks procedure has been developed to solve a single-point problem, that refers to the relation of input forces and output displacements considered at the same point [46].

An alternative framework, based on projective geometry, has been introduced for the analysis of compliant systems in Ref.[47]. This framework relies on the antiprojective polarity properties of a unique conic section, that is the *ellipse of elasticity*. This ellipse can be associated to any elastic suspension, regardless of the complexity of its underlying topology [48]. The introduction of the projective plane, associated to the scalar field representing the compliance of the system, leads to a formulation able to capture the kinetostatics of the suspension, avoiding the limitations of the single-point condition. More specifically, the ellipse of elasticity embodies the antiprojective polarity transformation between lines of action and poles of displacements, extending single-point relations to single-body relations.

In this paper, a novel method for the synthesis of planar compliant mechanisms is presented. The *projective synthesis method* exploits the projective properties of the ellipses of elasticity for designing compliant systems that meet specific requirements, assigned in terms of both load–displacement relations and topological structure.

The method is based on a *top-down* procedure that starts from the design requirements and completes in the definition of the kinetostatic features of the elastic elements. More specifically, the first step consists of defining a primary ellipse that prescinds from the physical structure of the elastic suspension, and depends only on the load–displacement requirements. This ellipse is decomposed into secondary ellipses that represent substructures in series and parallel arrangements. This step can be iterated until the required topology is obtained. Eventually, the lowest-level ellipses are materialized into elastic elements, connected through a pattern of rigid links that defines the final compliant mechanism.

With respect to the other approaches presented in Literature, the projective synthesis method:

- relies on a geometric framework described only by one entity, that is the ellipse of elasticity;
- does not focus on the compliance of a single point, but allows the designer to define the 3-DoF compliance features of the output port body of the mechanism, and of all its two-port substructures;
- guarantees the fulfillment of all the design requirements;
- intrinsically guarantees the positive definiteness of the kinetostatic relations associated to all the substructures, since it is based on weighted projective geometry;
- is able to generate multiple equivalent solutions starting from the same requirements. This feature can be exploited to avoid mechanical interference and meet secondary or off-design issues, as motion of intermediate links, manufacturing, or footprint requirements;
- does not strictly require the implementation of optimization algorithms or refinement steps, or the design of a corresponding rigid-body mechanism.

The remainder of the manuscript is organized as follows. In Section 2, the synthesis problem and the synthesis procedure are introduced. The definition of the primary ellipse and its decomposition according to series and parallel arrangements are described in Sections 3 and 4, respectively. A possible materialization of the lowest-level ellipses and the definition of the physical structure of the mechanism are presented in Sections 5 and 6, respectively. Several examples of implementation of the method, and the corresponding numerical analyses, are presented in Section 7. Conclusions are reported in Section 8.

2. Problem statement

The synthesis at the mechanism level consists of designing an elastic suspension $\mathcal{L}_0$ able to meet the motion requirements on the moving body T. Generally, the requirements are assigned as load–displacement relations formulated in terms of compliance matrices. In case of planar systems, the compliance matrix is symmetric, $\boldsymbol{C} \in Sym_3(\mathbb{R})$, positive definite, $\sigma(\boldsymbol{C}) \in \mathbb{R}^+$, and it relates generalized forces $\boldsymbol{l} = \{\boldsymbol{f}, m\}^T$ to generalized displacements $\boldsymbol{s} = \{\boldsymbol{\delta}, \theta\}^T$. Every applied load can be reduced to a force $\boldsymbol{f}$, with line of action p belonging to the projective plane $\mathbb{P}_2$. Pure moments can be considered as zero-magnitude forces, with improper line of action p_∞ lying at infinity. Analogously, $\boldsymbol{s}$ belongs to a field of displacements defined by the pole $P \in \mathbb{P}_2$ and by the rotation θ. Pure translations can be considered as zero-magnitude rotations around improper poles $P_\infty \in p_\infty$. This scenario is depicted in Fig. 1(a).

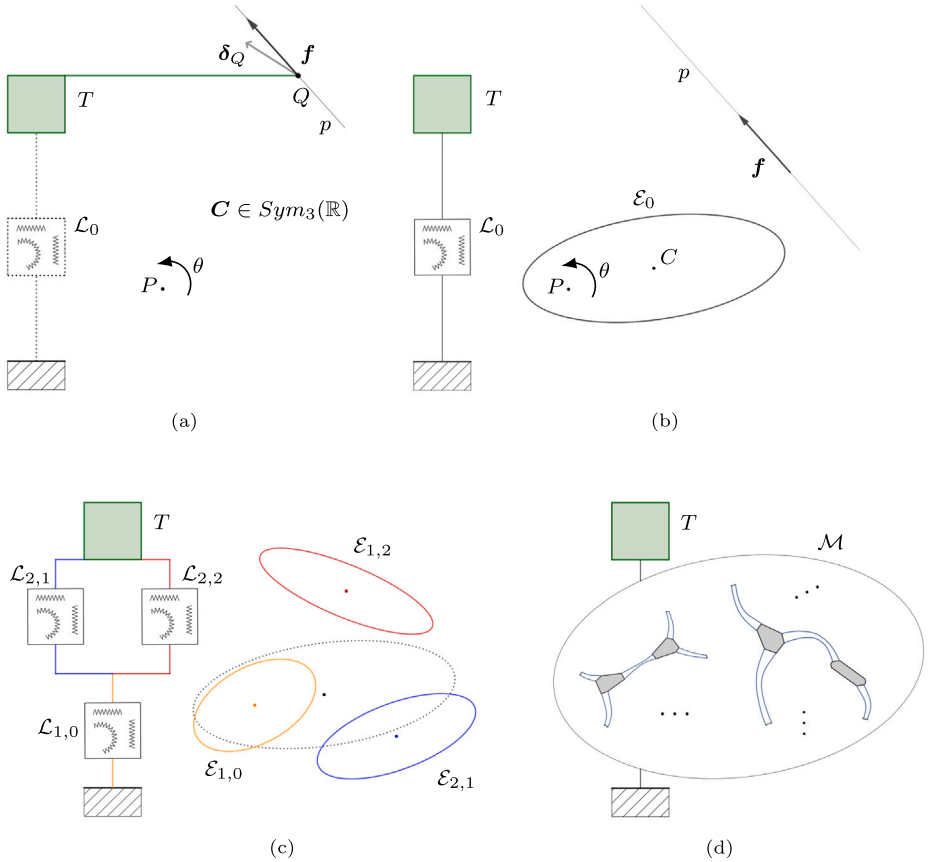

Fig. 1. Layout of the design procedure: requirements on the elastic suspension $\mathcal{L}_0$ (a), definition of the primary ellipse of elasticity $\mathcal{E}_0$ (b), decomposition into n–ary ellipses of elasticity (c), and materialization of the flexures and of the rigid connections defining the compliant mechanism $\mathcal{M}$(d).

The load–displacement relations described above, besides the formulation in terms of compliance matrices $\boldsymbol{C}$, can be described in terms of projective geometry. In both cases, they can be represented by the *ellipse of elasticity* $\mathcal{E}_0$, as shown in Fig. 1(b). This model consists of a conic section and an associated elastic weight w, that embody the bijective correspondence between lines p and points P, and the compliance of the relations, respectively. The ellipse $\mathcal{E}_0$ represents load–displacement relations through its projective geometry features. More specifically, the line p is the line of action of the resulting applied load, and the point P is the pole of the displacements of the body, also defined as center of rotation. Therefore, this model converts the kinetostatic problem into a geometrical one [47,48]. Additionally, analogously to the ellipse of inertia of a continuum distribution of mass, $\mathcal{E}_0$ is the momental ellipse of a continuum distribution of elastic weights.

As a consequence, the ellipse of elasticity can be materialized into an elastic suspension. This step depends on the topological requirements on the system.

In the simplest case, the ellipse $\mathcal{E}_0$ is actualized as a single elastic element. However, to meet the required topology, a more complex arrangement of ellipses can be considered, according to a *top-down* approach. More specifically, the primary ellipse $\mathcal{E}_0$ can be decomposed into a series or into a parallel arrangement of secondary ellipses. This procedure can be systematically iterated, to obtain secondary, ternary, n-ary ellipses, as depicted in Fig. 1(c).

Eventually, at the lowest levels, the ellipses are materialized into elastic elements that, arranged according to the assigned topology through rigid connections, define the compliant mechanism $\mathcal{M}$, as shown in Fig. 1(d).

Therefore, the input data of the problem are the load–displacement requirements and, possibly, the system topology, defined as series and parallel substructures. Then, the synthesis procedure at the mechanism level can be summarized as follows.

1. Definition of the primary ellipse of elasticity $\mathcal{E}_0$, considering the load–displacement requirements.
2. Decomposition of the primary ellipse into n-ary ellipses, according to the topology.
3. Materialization of the lowest-level ellipses in elastic elements.
4. Rigid connection of the elastic elements.

The synthesis steps are discussed in detail in the next sections. It is worth noting that the execution of steps (2), (3), and (4), comprises several arbitrary design choices. This fact leads to multiple solutions to the synthesis problem that are equivalent from

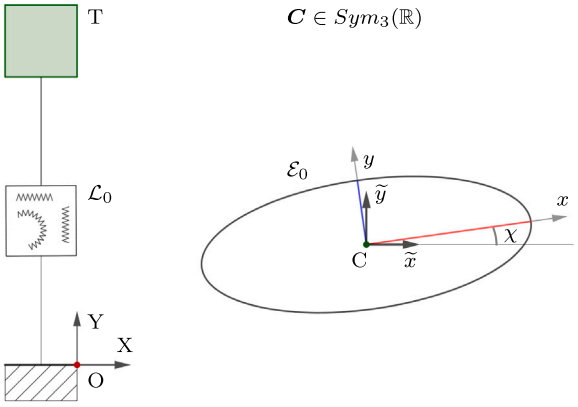

Fig. 2. Ellipse of elasticity $\mathcal{E}_0$ obtained from a compliance matrix $\boldsymbol{C}$.

the kinetostatic point of view. This multiplicity can be exploited to meet secondary or off-design issues, as manufacturing, footprint, or motion of the intermediate links requirements. This point is discussed in the next sections.

3. Definition of the primary ellipse

Generally, the load–displacement relations can be expressed in several ways. In this paper, two different approaches are considered. The first one, commonly used in Literature, defines the load–displacement relation in terms of compliance matrices. The second one, based on the direct assignment of force directions and poles of displacements, is formulated in terms of projective geometry. The steps required to obtain the primary ellipse of elasticity, starting from the two different assignments, are described in the following subsections.

3.1. Definition of the primary ellipse from the compliance matrix

A load–displacement relation can be generally formulated in terms of a compliance matrix $\boldsymbol{C}$ defined with respect to a reference frame $R \equiv \{O, X, Y\}$. The ellipse of elasticity $\mathcal{E}_0$ can be determined by exploiting one of its fundamental properties, i.e. the decoupling of forces and moments at its center $C \equiv (X_C, Y_C)$.

With reference to Fig. 2, the matrix $\boldsymbol{C}$, in the translated reference frame $\widetilde{R} \equiv \{C, \widetilde{x}, \widetilde{y}\}$, becomes

$$\widetilde{\boldsymbol{C}}_0 = \boldsymbol{T}^T \boldsymbol{C} \boldsymbol{T}\,, \tag{1}$$

where

$$\boldsymbol{T} = \begin{bmatrix} 1 & 0 & 0 \\ 0 & 1 & 0 \\ -Y_C & X_C & 1 \end{bmatrix}. \tag{2}$$

The entry $\boldsymbol{C}(3,3)$, called *elastic weight* w, relates the rotation and the pure moment as

$$w = \boldsymbol{C}(3,3) = \widetilde{\boldsymbol{C}}_0(3,3) = \frac{\boldsymbol{M}}{\theta}\,, \tag{3}$$

and it is invariant with respect to the transformation represented by Eq. (1). Since forces with line of action through C produce pure translations, it follows

$$\widetilde{\boldsymbol{C}}_0(3,1) = \widetilde{\boldsymbol{C}}_0(3,2) = 0\,. \tag{4}$$

Then, from Eqs. (1) and (4), the coordinates of the center of the ellipse are obtained as

$$X_C = -\frac{\boldsymbol{C}(3,2)}{w}\,, \quad Y_C = \frac{\boldsymbol{C}(3,1)}{w}\,. \tag{5}$$

Once the center has been determined, another fundamental property of the ellipse can be exploited, i.e. forces with lines of action overlapping the ellipse semi-axes produce pure translations along the same direction. As a consequence, the reference frame $R' \equiv \{C\, x\, y\}$ can be introduced, where x and y overlap the semi-axes of the ellipse a and b, respectively. The angle χ defines the orientation of R' with respect to $\widetilde{R}$. Therefore, in R', the matrix $\widetilde{\boldsymbol{C}}_0$ takes the diagonal form

$$\boldsymbol{C}_0 = w \begin{bmatrix} b^2 & 0 & 0 \\ 0 & a^2 & 0 \\ 0 & 0 & 1 \end{bmatrix}. \tag{6}$$

Through the relations Eqs. (3), (5) and (6), the geometric parameters of the ellipse, X_C, Y_C, a, b, and χ, and its associated elastic parameter w, are determined.

3.2. Definition of the primary ellipse in terms of projective geometry

In terms of projective geometry, the load–displacement relations are formulated by assigning lines of action and corresponding poles of displacements. However, considering an elastic system in neutral configuration, these assignments cannot be completely arbitrary. More specifically, the loads must satisfy the Maxwell's reciprocal theorem [49] (i), and every linear combination of them must do a positive work (ii). It is worth noting that the mechanical conditions (i) and (ii) correspond to the symmetric form and to the positive definiteness, respectively, of the compliance matrix discussed in Section 3.1.

A system of lines of action and poles that satisfies the previous conditions is represented in Fig. 3(a). Since the force $\boldsymbol{f}_i$ passes through the poles P_j and P_k, its reciprocal work is always zero, whereas its work on the field of displacements defined by P_i is always positive. In the projective plane $\mathbb{P}_2$, the point P_i and the line p_i can be considered as the antipole and the antipolar, respectively, of the antiprojective polarity transformation defined by the ellipse $\mathcal{E}_0$. A triangle whose each vertex and corresponding opposite side is a pair of antipole and antipolar, respectively, is defined as a *self-polar triangle* associated to $\mathcal{E}_0$, and it can be exploited to determine the conic parameters. In fact, when each vertex of the self-polar triangle is associated to an elastic weight, the *weighted self-polar triangle* is univocally associated to its momental ellipse, that is the ellipse of elasticity. More specifically, the elastic weights are defined as

$$w_i = \frac{\vartheta_i}{M_i}, \tag{7}$$

where

$$\boldsymbol{m}_i = \overrightarrow{P_i P}_{j\neq i} \times \boldsymbol{f}_i \tag{8}$$

is the moment of $\boldsymbol{f}_i$ with respect to the opposite pole. The distribution has total elastic weight

$$w = \sum w_i \,. \tag{9}$$

With reference to Fig. 3(b), the point Q_i is the barycenter of the system of the weighted points P_j and P_k,

$$\overline{Q_i P_j} w_j = \overline{O_i P_k} w_k \,, \tag{10}$$

and

$$\overline{CQ_i}(w - w_i) = \overline{CP_i} w_i \,. \tag{11}$$

The barycenter of the system, that is the ellipse center C, is obtained from Eqs. (10) and (11). It can be noted that C is always located inside the triangle. The particular cases of C belonging to the sides or coincident one vertex are discussed in Section 3.3.

Finally, according to the antiprojective polarity properties, the points E_i belonging to the ellipse can be found as

$$\overline{CE_i}^2 = \overline{CQ_i}\,\overline{CP_i} \,. \tag{12}$$

Once the points C and E_i, and the elastic weight w are determined, the ellipse $\mathcal{E}_0$ is completely defined.

3.3. Particular cases

The assigned requirements can lead to the definition of particular ellipses of elasticity.

The first case consists of an ellipse with eccentricity $e = 1$, that is a circle. In terms of compliance matrix, it means that the eigenvalues of the upper-left 2×2 block of $\widetilde{\boldsymbol{C}}_0$ are equal. In terms of projective geometry, the center of the ellipse is coincident to the orthocenter of the self-polar triangle, as depicted in Fig. 4.

The second case consists of an ellipse with eccentricity $e = 0$, that is a line segment. The upper-left 2×2 block of $\widetilde{\boldsymbol{C}}_0$ has rank 1, since the compliance along the line is zero. In terms of projective geometry, the weight associated to one vertex of the self-polar triangle is zero, and the ellipse degenerates into a segment lying on the opposite side, as depicted in Fig. 5.

The third case consists of an ellipse degenerated into a point. The upper-left 2×2 block of $\widetilde{\boldsymbol{C}}_0$ has rank 0 and the compliance along all directions is zero. The weight associated to two vertices of the self-polar triangle is zero, and the ellipse degenerates into a point coincident to the third vertex.

4. Decomposition of the primary ellipse into n-ary ellipses

The primary ellipse $\mathcal{E}_0$ is decomposed into two secondary ellipses connected in series or in parallel arrangements. As described in the next subsections, the decomposition can be performed by exploiting the relations between ellipses and self-polar triangles. More specifically, every ellipse can be associated to ∞^3 triangles, whereas every set of a primary and two secondary ellipses is associated to a unique triangle [50]. According to a top-down approach, the secondary ellipses can be further decomposed to obtain the final required topology.

The first step of the decomposition, both in case of series or parallel arrangement, consists of determining one weighted self-polar triangle associated to $\mathcal{E}_0$. If the synthesis requirements are given in terms of projective geometry, the triangle defined in Section 3.2 can be considered. In general, a weighted self-polar triangle $\mathcal{T}$, with vertices P_i, can be defined, with reference to Fig. 6, as follows.

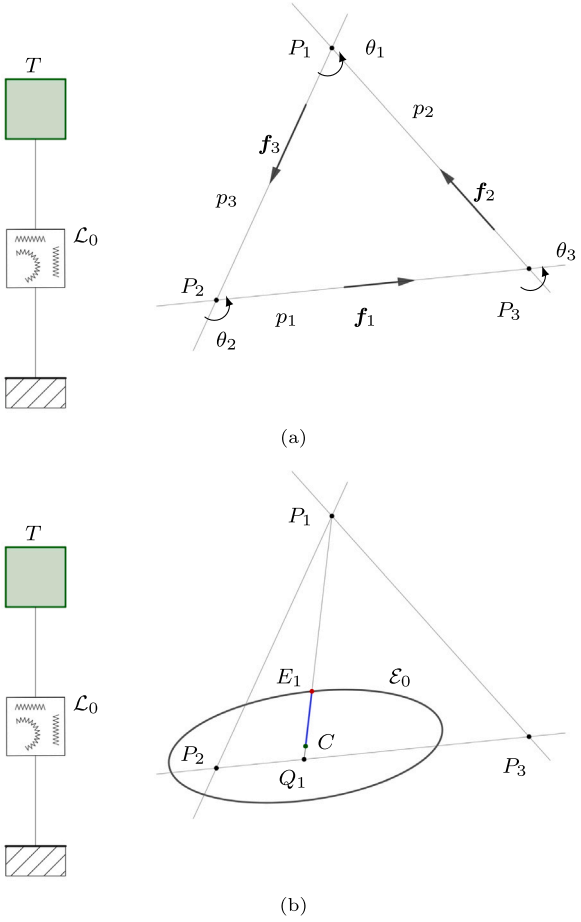

Fig. 3. Forces and poles defining a self-polar triangle (a) and corresponding ellipse of elasticity.

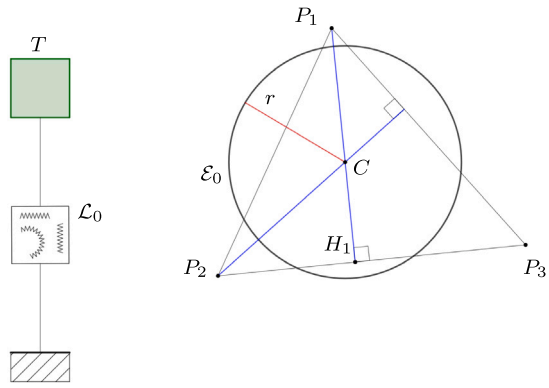

Fig. 4. Ellipse with eccentricity $e = 1$: the center is coincident to the orthocenter of the self-polar triangle, and $r^2 = \overline{CP_i}\,\overline{CH_i}$.

1. Choose an arbitrary point P_1 and find its antipolar p_1 with respect to $\mathcal{E}_0$. More specifically, the point E_1 is first determined by the intersection between the ellipse and the line d_1 passing through P_1 and C. The t_1 is the tangent to the ellipse in E_1. Then, the point $Q_1 \in d_1$, that is the elliptic inverse point of P_1, is determined according to Eq. (12). The line p_1, passing through Q_1 and parallel to t_1, is the antipolar of P_1.
2. Choose an arbitrary point P_2 belonging to p_1. By following the procedure described in the previous point, find its antipolar p_2.
3. Find P_3 as the intersection of p_1 and p_2.

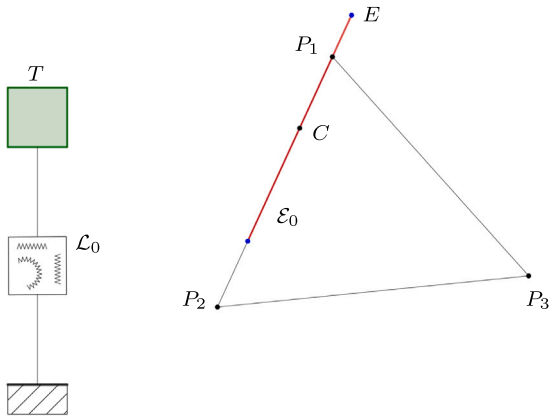

Fig. 5. Ellipse with eccentricity $e = 0$: $w_3 = 0$, $\overline{CE}^2 = \overline{CP_1}\,\overline{CP_2}$.

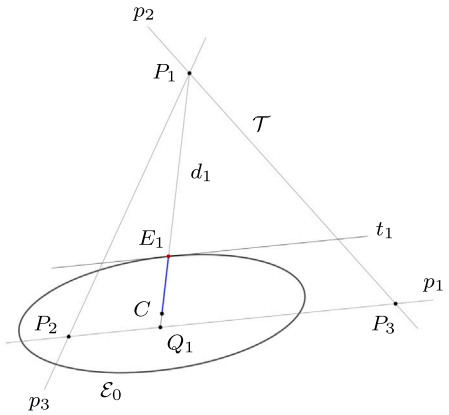

Fig. 6. Construction of the self-polar triangle $\mathcal{T}$ associated to the ellipse $\mathcal{E}_0$.

4. Find the elastic weights associated to the points. According to Eqs. (11) and (12), the elastic weights are

$$w_i = \frac{\overline{CE_i}^2}{\overline{CE_i}^2 + \overline{CP_i}^2} w\,. \tag{13}$$

The weighted self-polar triangle $P_1P_2P_3$ can be exploited for the decomposition in series or in parallel arrangements.

4.1. Series decomposition

If the elastic suspension $\mathcal{L}_0$ must be decomposed in the series arrangement of $\mathcal{L}_{s_1}$ and $\mathcal{L}_{s_2}$, the primary ellipse $\mathcal{E}_0$ must be decomposed into the secondary ellipses $\mathcal{E}_{s_1}$ and $\mathcal{E}_{s_2}$, associated to $\mathcal{L}_{s_1}$ and $\mathcal{L}_{s_2}$, respectively. The weighted self-polar triangle $\mathcal{T}$ with vertices P_i, associated to the primary ellipse, can be exploited to define the secondary ellipses. In fact, with reference to Fig. 7, the secondary ellipses can be represented by the same self-polar triangle, but with different *weights*. More specifically, the elastic weights relative to the secondary ellipses must satisfy the following conditions.

1. Every secondary ellipse must have positive elastic weights associated to the vertices of the triangle.
2. For every vertex, the sum of the compliances of the secondary ellipses must be equal to the compliance of the primary ellipse.

Both conditions are met if, for each pole P_i,

$$w_{s_{1,i}} = \mu_{1,i}\, w_i\,, \tag{14}$$

$$w_{s_{2,i}} = \mu_{2,i}\, w_i\,, \tag{15}$$

where

$$\mu_{2,i} = 1 - \mu_{1,i}\,, \quad 0 < \mu_{1,i},\, \mu_{2,i} < 1\,, \tag{16}$$

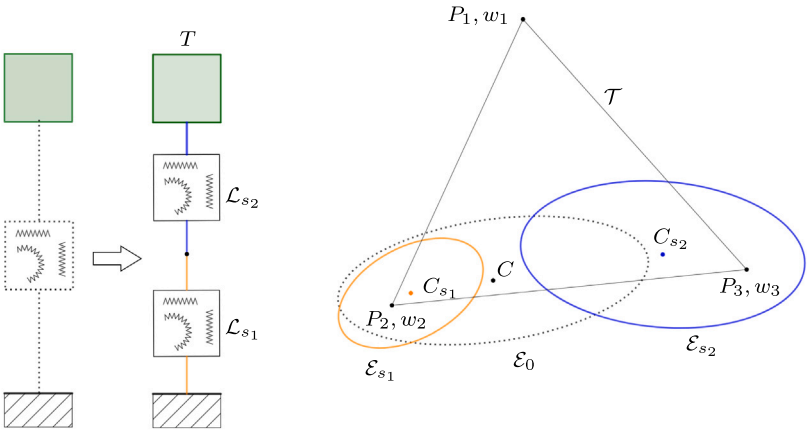

Fig. 7. Series decomposition, $w_i = w_{s_{1,i}} + w_{s_{2,i}}$, $i = 1, 2, 3$, with $\{\mu_{1,1}, \mu_{1,2}, \mu_{1,3}\} = \{0.475, 0.913, 0.065\}$.

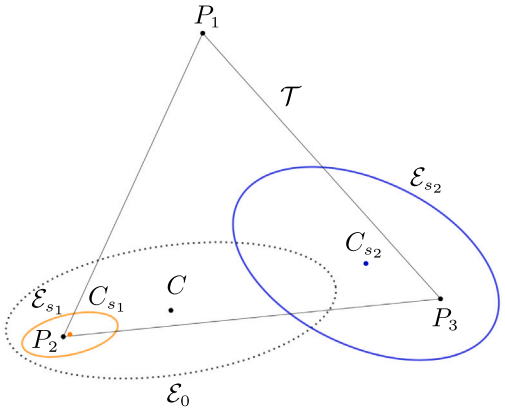

Fig. 8. Series decomposition, $w_i = w_{s_{1,i}} + w_{s_{2,i}}$, $i = 1, 2, 3$, with $\{\mu_{1,1}, \mu_{1,2}, \mu_{1,3}\} = \{0.064, 0.948, 0.057\}$.

and $w_{s_{1,i}}$ and $w_{s_{2,i}}$ are the elastic weights associated to the point P_i of $\mathcal{E}_{s_1}$ and $\mathcal{E}_{s_2}$, respectively. In this case, the condition

$$w = w_{s_1} + w_{s_2} \tag{17}$$

is guaranteed. Once the secondary weighted self-polar triangles are defined, the secondary ellipses can be determined according to the procedure described in Section 3.2. The decomposition of the primary ellipse, performed the values $\{\mu_{1,1}, \mu_{1,2}, \mu_{1,3}\} = \{0.475, 0.913, 0.065\}$, is shown in Fig. 7.

From Eqs. (14) and (15), different sets of values of $\mu_{1,i}$, $\mu_{2,i}$ lead to differently weighted self-polar triangles associated to $\mathcal{E}_{s_1}$ and $\mathcal{E}_{s_2}$. As a consequence, different decompositions of $\mathcal{E}_0$ can be obtained. For example, the decomposition corresponding to the values $\{\mu_{1,1}, \mu_{1,2}, \mu_{1,3}\} = \{0.064, 0.948, 0.057\}$ is depicted in Fig. 8.

It is worth noting that, in the cases above, a generic self-polar triangle $\mathcal{T}$ has been considered. This choice leads to a configuration of secondary ellipses that are, in general, not equal and not symmetrically posed with respect to $\mathcal{E}_0$. However, a symmetric decomposition can be obtained by considering a symmetric weighted self-polar triangle. With reference to Fig. 9, $\mathcal{T}_{sym}$ is obtained, according to the procedure described above, by placing the vertex P_1 along one of the ellipse axis. By choosing the minor semi-axis, the triangle is symmetric with respect to b, therefore $w_2 = w_3$. To achieve symmetric decompositions, the weights of the secondary ellipses must be set symmetrically, as

$$\begin{aligned} w_{s_{1,1}} &= w_{s_{2,1}}\,, \\ w_{s_{1,2}} &= w_{s_{2,3}}\,, \\ w_{s_{1,3}} &= w_{s_{2,2}}\,. \end{aligned}$$

In other terms, the weight of $\mathcal{E}_{s_1}$ in P_2 must be equal to the weight of $\mathcal{E}_{s_2}$ in P_3, and viceversa.

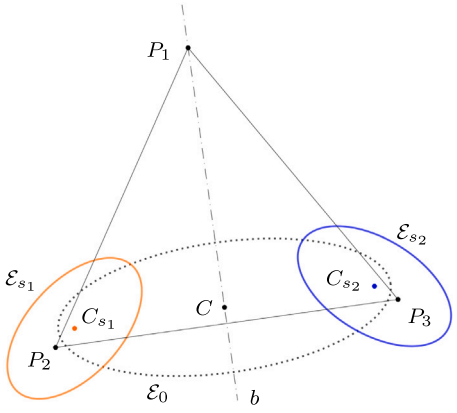

Fig. 9. Symmetric series decomposition, $w_i = w_{s_{1,i}} + w_{s_{2,i}}$, $i = 1, 2, 3$, with $\{\mu_{1,1}, \mu_{1,2}, \mu_{1,3}\} = \{0.500, 0.965, 0.035\}$.

4.2. Parallel decomposition

In case of parallel arrangement, the elastic suspension $\mathcal{L}_0$ must be decomposed in the suspensions $\mathcal{L}_{p_1}$ and $\mathcal{L}_{p_2}$. Therefore, the primary ellipse $\mathcal{E}_0$ must be decomposed into the secondary ellipses $\mathcal{E}_{p_1}$ and $\mathcal{E}_{p_2}$, associated to $\mathcal{L}_{p_1}$ and $\mathcal{L}_{p_2}$, respectively, as depicted in Fig. 10. Analogously to the series case, the secondary ellipses are represented by the same self-polar triangle, with different weights, satisfying the following conditions.

1. Every secondary ellipse must have positive elastic weights associated to the vertices of the triangle.
2. For every vertex, the sum of the stiffnesses of the secondary ellipses must be equal to the stiffness of the primary ellipse.

Both conditions are met if, for each pole P_i,

$$\frac{1}{w_{p_{1,i}}} = \nu_{1,i} \frac{1}{w_i}\,, \tag{18}$$

$$\frac{1}{w_{p_{2,i}}} = \nu_{2,i} \frac{1}{w_i}\,, \tag{19}$$

where

$$\nu_{2,i} = 1 - \nu_{1,i}\,, \quad 0 < \nu_{1,i}, \nu_{2,i} < 1\,, \tag{20}$$

and $w_{p_{1,i}}$ and $w_{p_{2,i}}$ are the elastic weights associated to the point P_i of $\mathcal{E}_{p_1}$ and $\mathcal{E}_{p_2}$, respectively. It is worth noting that, in this case, the condition on the reciprocal elastic weights results in

$$\frac{1}{w} \geq \frac{1}{w_{p_1}} + \frac{1}{w_{p_2}}\,. \tag{21}$$

Once the secondary weighted self-polar triangles are defined, the secondary ellipses can be determined according to the procedure described in Section 3.2.

Analogously to Eqs. (14) and (15) in the series case, different sets of values of $\nu_{1,i}$, $\nu_{2,i}$ in Eqs. (18) and (19) lead to different decompositions of $\mathcal{E}_0$. For example, the decompositions obtained with the values $\{\nu_{1,1}, \nu_{1,2}, \nu_{1,3}\} = \{0.999, 0.554, 0.149\}$ and $\{\nu_{1,1}, \nu_{1,2}, \nu_{1,3}\} = \{0.993, 0.146, 0.679\}$ are depicted in Figs. 10 and 11, respectively.

In case of a symmetry requirement, a symmetric weighted self-polar triangle can be considered, as in the series case. More specifically,

$$\frac{1}{w_{p_{1,1}}} = \frac{1}{w_{p_{2,1}}}\,,$$
$$\frac{1}{w_{p_{1,2}}} = \frac{1}{w_{p_{2,3}}}\,,$$
$$\frac{1}{w_{p_{1,3}}} = \frac{1}{w_{p_{2,2}}}\,.$$

In other terms, the reciprocal elastic weight of $\mathcal{E}_{s_1}$ in P_2 must be equal to the reciprocal elastic weight of $\mathcal{E}_{s_2}$ in P_3, and viceversa. The decomposition with $\{\nu_{1,1}, \nu_{1,2}, \nu_{1,3}\} = \{0.500, 0.046, 0.954\}$ is illustrated in Fig. 12.

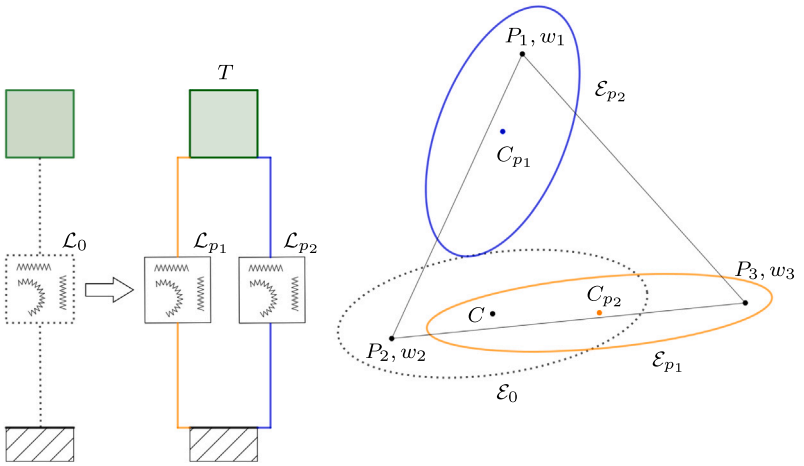

Fig. 10. Parallel decomposition, $1/w_i = 1/w_{p_{1,i}} + 1/w_{p_{2,i}}$, $i = 1, 2, 3$, with $\{\nu_{1,1}, \nu_{1,2}, \nu_{1,3}\} = \{0.999, 0.554, 0.149\}$.

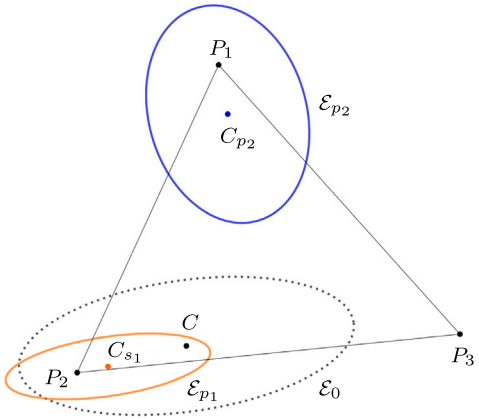

Fig. 11. Parallel decomposition, $1/w_i = 1/w_{p_{1,i}} + 1/w_{p_{2,i}}$, $i = 1, 2, 3$, with $\{\nu_{1,1}, \nu_{1,2}, \nu_{1,3}\} = \{0.993, 0.146, 0.679\}$.

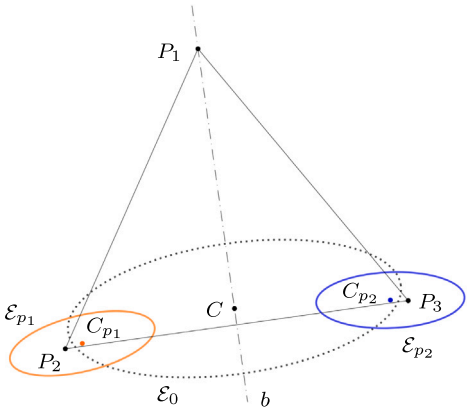

Fig. 12. Symmetric parallel decomposition, $1/w_i = 1/w_{p_{1,i}} + 1/w_{p_{2,i}}$, $i = 1, 2, 3$, with $\{\nu_{1,1}, \nu_{1,2}, \nu_{1,3}\} = \{0.500, 0.046, 0.954\}$.

5. Materialization of the lowest-level ellipses in elastic elements

Once the lowest-level ellipses have been determined according to the topological requirements, the third step of the procedure consists of the synthesis *at the element level*, that is the design of the elastic elements that correspond to the defined ellipses.

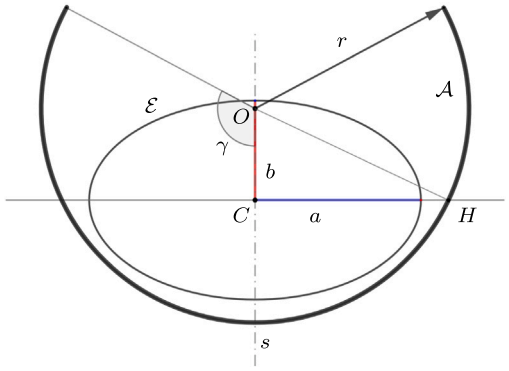

Fig. 13. Uniform arc $\mathcal{A}$ associated to the ellipse $\mathcal{E}$ with eccentricity $e = a/b = 0.6$.

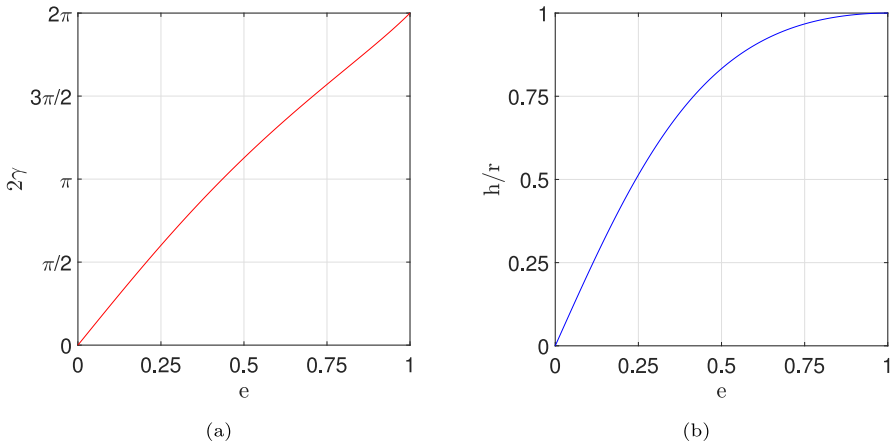

Fig. 14. Trends of the angle 2γ (a) and of the ratio h/r (b) with respect to the eccentricity.

This step belongs to the general problem of finding or optimizing shape, size, and material properties of a continuum under a set of constraints. This problem is generally not trivial and has been addressed in several investigations [51–56]. Therefore, a general and in-depth treatment of the problem is out of the scope of this article. However, focusing on the association of an ellipse of elasticity to an elastic element, the problem can be solved, in a general way, by resorting to families of flexures with defined ellipses. For instance, the relations of the geometric parameters of circular and parabolic arcs with the ones of the corresponding ellipses, determined in closed form in Ref. [48], can be exploited. Therefore, in this investigation, uniform circular arcs are adopted without loss of generality. With reference to Fig. 13, the problem is formulated as follows:

> given an ellipse $\mathcal{E}$ with parameters a, b, and w, find the corresponding circular arc defined by radius of curvature r, subtending angle 2γ, and flexural rigidity EI. Find also its pose with respect to the ellipse.

The beam axis of symmetry s overlaps the ellipse minor semi-axis b, whereas the distance of the arc center O from the ellipse center C is expressed by

$$\overline{OC}^2 = r^2 - h^2 = r^2 \frac{\sin(\gamma)^2}{\gamma^2}, \tag{22}$$

where $h \equiv \overline{CH} = \sqrt{a^2 + b^2}$. Also, r and γ are related to the length of the major semi-axis a by the expression

$$a^2 = \frac{r^2}{2}\left(1 - \frac{sin(2\gamma)}{2\gamma}\right). \tag{23}$$

Making use of Eqs. (22) and (23), the values r, γ, and $\overline{OC}$ can be computed from the ellipse parameters a and b. The trends of the angle 2γ and of the ratio h/r with respect to the eccentricity e are shown in Fig. 14(a) and (b), respectively. As it can be noted from the figures, real solutions exist for every value of a and of b.

Two examples of arcs $\mathcal{A}$ determined from their ellipses $\mathcal{E}$ are shown in Fig. 15(a) and in Fig. 15(b), in case of eccentricity $e = 0.3$ and $e = 0.9$, respectively.

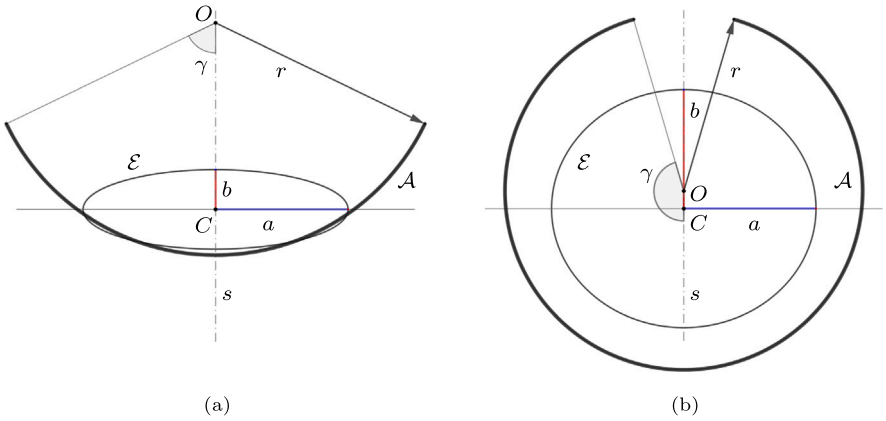

Fig. 15. Arcs $\mathcal{A}$ associated to ellipses $\mathcal{E}$ with eccentricity $e = 0.3$ (a) and $e = 0.9$ (b).

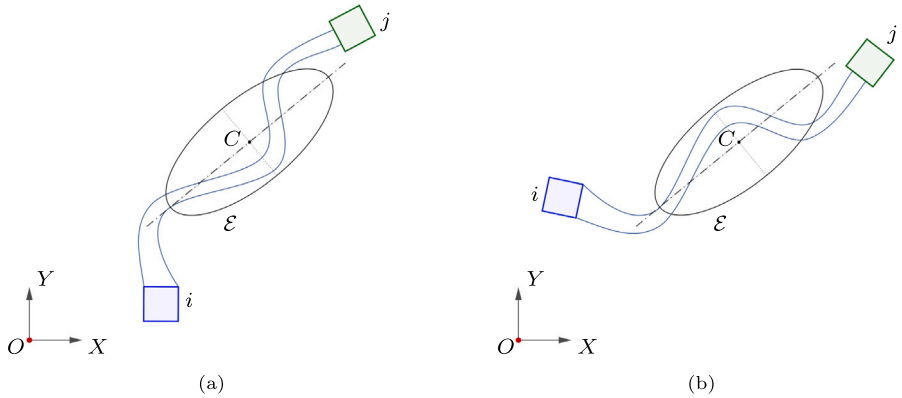

Fig. 16. Equivalent poses: the flexure in Fig. 16(b) is obtained by flipping the flexure in Fig. 16(a) around the major semi-axis of the ellipse.

In the particular case of $e = 0$, the ellipse degenerates into a line segment, as discussed in Section 3.3. The associated flexure becomes a straight-axis beam with length $l = 2a\sqrt{3}$. For $e = 1$, the ellipse becomes a circle, and its associated flexure is a full-angle ring beam with radius $a\sqrt{2}$ and center coincident to the center of the ellipse.

Finally, the geometry of the beam cross-sections can be established considering the flexural rigidity, as

$$EI = \frac{2r\gamma}{w}, \tag{24}$$

where E is the Young's modulus and I is the second moment of area of the cross-section.

Through Eqs. (22) to (24) every ellipse can be materialized into an elastic element, concluding the top-down procedure.

It is worth noting that the elastic element, given the pose on the plane of its ellipse, can be positioned in different ways. In fact, every ellipse, if reflected around its semi-axes or rotated by π around its center, overlaps itself. The same operations, performed on the elastic element, result in different poses with equivalent linear kinetostatic behavior. In Fig. 16, the pose of the ellipse is defined with respect to the reference $R \equiv \{O, X, Y\}$. The flexure in Fig. 16(b) is obtained by flipping flexure in Fig. 16(a) around the major semi-axis. The two systems have equivalent linear behavior, with the same relative center of rotation between the bodies i and j and the same relative field of displacements. This feature can be exploited to optimize the final layout of the compliant mechanism.

6. Rigid connection of the elastic elements

The last phase of the synthesis procedure consists of defining the rigid-body connections among the elastic elements, according to the assigned topology. However, once the lowest-level ellipses have been determined and the corresponding flexures have been positioned, the connections are not uniquely defined. As discussed in the previous section about the flexure positioning, this feature can be exploited to reduce footprint area, avoid mechanical interference, cope with manufacturing issues or internal motion requirements.

Table 1
Geometric and elastic parameters of the open-chain compliant mechanism and of its corresponding ellipses of elasticity. Angles in radians, lengths in millimeters, flexural rigidities in N mm^2. The angle σ defines the orientation of the arc bisector with respect to the x-axis.

Self-polar Triangle											
P_1				P_2				P_3			
x	y	w_i/w	μ_1	x	y	w_i/w	μ_1	x	y	w_i/w	μ_1
14.79	34.03	0.154	0.563	−28.24	−2.19	0.435	0.850	24.38	−10.43	0.411	0.008
Secondary ellipses of elasticity											
$\mathcal{E}_1$						$\mathcal{E}_2$					
x_C	y_C	a	b	χ	w_S/w	x_C	y_C	a	b	χ	w_S/w
−19.74	4.57	22.07	3.46	0.68	0.46	23.14	−5.35	14.45	2.71	−1.35	0.54
Compliant mechanism											
$\mathcal{A}_1$						$\mathcal{A}_2$					
x_O	y_O	r	σ	γ	EI	x_O	y_O	r	σ	γ	EI
−58.99	52.68	65.99	−0.89	0.60	367.7	56.02	2.10	26.79	0.22	0.72	286.5

An example of different connection patterns is shown in Fig. 17. The primary ellipse $\mathcal{E}_0$ is decomposed into the parallel arrangement $\mathcal{E}_{1,0}$ and $\mathcal{E}_{1,0}$. The ellipse $\mathcal{E}_{1,0}$ represents the flexure $\mathcal{F}_{1,0}$ connecting the body T to the ground, whereas $\mathcal{E}_{2,0}$ represents the series composed by the flexures $\mathcal{F}_{2,1}$ and $\mathcal{F}_{2,2}$, and by the rigid body k. In Fig. 17(a), T is connected to the ground through the patterns of rigid cross-sections $s_1 - s_3 - s_4$ for the left limb, and $s_2 - s_5 - s_6 - s_7 - s_8$ for the right limb. In Fig. 17(b), the patterns are $s_1 - s_4 - s_3$ for the left limb and $s_2 - s_7 - s_8 - s_5 - s_6$ for the right limb.

Considering the linear kinetostatic behavior of the body T, the two connection patterns are equivalent. However, the patterns result in a different behavior of the body k. In fact, the ellipse $\mathcal{E}_{2,0}$ represents the relative load–displacement relation of the right limb, between s_2 and the ground, regardless of the lower-level topology and connections.

Generally, this feature can be exploited to address secondary requirements in terms of motion of the intermediate bodies.

7. Applications

The proposed procedure has been implemented for the solution of the synthesis problems defined by the following requirements expressed, equivalently, both in terms of projective geometry and of compliance matrix, according to Sections 3.1 and 3.2.

1. Primary ellipse $\mathcal{E}_0$ with eccentricity $e = 0.6$ ($a = 25$ mm, $b = 15$ mm), elastic weight $w = 0.4$ rad(N mm)$^{-1}$, and open-chain topology consisting of two flexures and of two rigid bodies;

$$\boldsymbol{C}_0 = \begin{bmatrix} 90.00 & 0 & 0 \\ 0 & 250.00 & 0 \\ 0 & 0 & 0.400 \end{bmatrix}. \tag{25}$$

2. Primary ellipse $\mathcal{E}_0$ with eccentricity $e = 0.6$ ($a = 25$ mm, $b = 15$ mm), elastic weight $w = 0.0157$ rad(N mm)$^{-1}$, and closed-chain topology consisting of two flexures and of one rigid body.

$$\boldsymbol{C}_0 = \begin{bmatrix} 3.53 & 0 & 0 \\ 0 & 9.80 & 0 \\ 0 & 0 & 0.0157 \end{bmatrix}. \tag{26}$$

In Eqs. (25) and (26), the unit of the entries $\boldsymbol{C}_0(1,1)$ and $\boldsymbol{C}_0(2,2)$ is mm(N)$^{-1}$, whereas the unit of the entry $\boldsymbol{C}_0(3,3)$ is rad(N mm)$^{-1}$.

7.1. Open-chain compliant mechanism

Starting from the requirements (1), the synthesis is performed according to the procedure described in Section 4.1, considering an asymmetric decomposition. The primary ellipse, the common self-polar triangle, and the secondary ellipses are depicted in Fig. 18(a). The corresponding flexures, materialized as circular arcs, have been obtained as described in Section 5. The compliant mechanism is shown in Fig. 18(b), whereas the geometric and elastic parameters of the self-polar triangle, of the ellipses, and of the flexures, are listed in Table 1.

To verify the synthesis procedure, finite element analyses have been conducted with the commercial software Nastran. Three different load conditions have been considered, consisting of a pure moment $\boldsymbol{m}$ applied on T, and of two forces, $\boldsymbol{f}_x$ and $\boldsymbol{f}_y$, with lines of action parallel to the semi-axes a and b of the primary ellipse, respectively. The forces have been applied to a point Q rigidly connected to T and overlapping, in the unloaded configuration, the center C of the ellipse. Because of the antiprojective properties of the ellipse of elasticity, forces parallel to the semi-axes and passing through the center C are expected to produce pure

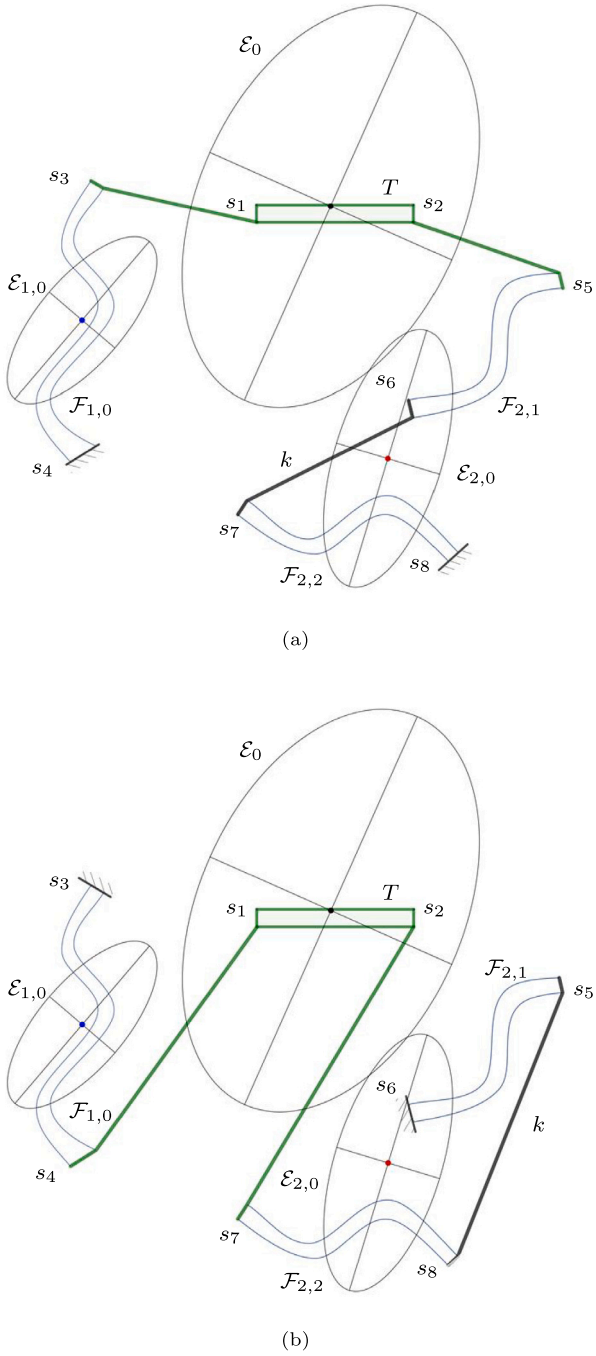

Fig. 17. Rigid connection of elastic elements: different connection patterns.

translations along the same axis direction, whereas pure moments are expected to produce pure rotations around C. With reference to Eq. (6), theoretical displacements and rotations can be calculated as:

$$\begin{aligned} \delta_x &= wb^2 f_x\,, \\ \delta_y &= wa^2 f_y\,, \\ \theta &= wm\,. \end{aligned} \tag{27}$$

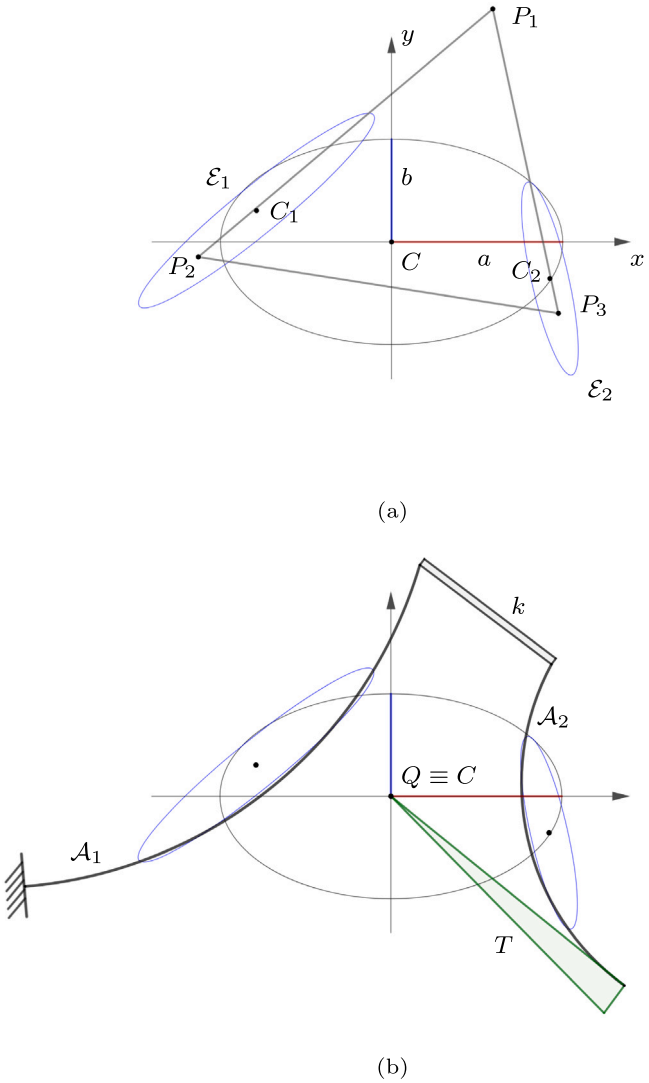

Fig. 18. Open-chain synthesis: primary ellipse, the common self-polar triangle, and the secondary ellipses (a), and materialized compliant mechanism (b).

Table 2
Open-chain compliant mechanism synthesis: generalized displacements obtained with the theoretical approach and with FEA simulations. Forces in Newton, lengths in millimeters, angles in radians.

Load		Theory			FEA		
Type	Magnitude	δ_x	δ_y	θ	δ_x	δ_y	θ
$\boldsymbol{f}_x$	0.1	9.00	0.00	0.000	8.99	0.00	0.000
$\boldsymbol{f}_y$	0.1	0.00	25.00	0.000	0.00	24.97	0.000
$\boldsymbol{m}$	1.0	0.00	0.00	0.400	0.00	0.00	0.400

The theoretical and the numerical results are reported in Table 2. FEA validate the theoretical predictions, since errors are below 0.2%.

7.2. Closed-chain compliant mechanism

Considering the requirements (2), the synthesis follows the steps described in Section 4.2. In this case, a symmetric decomposition is considered. The primary ellipse, the common self-polar triangle, and the secondary ellipses are depicted in Fig. 19(a). The corresponding flexures are, also in this case, materialized as circular arcs. The compliant mechanism is shown in Fig. 19(b), whereas the geometric and elastic parameters of the self-polar triangle, of the ellipses, and of the flexures are listed in Table 3.

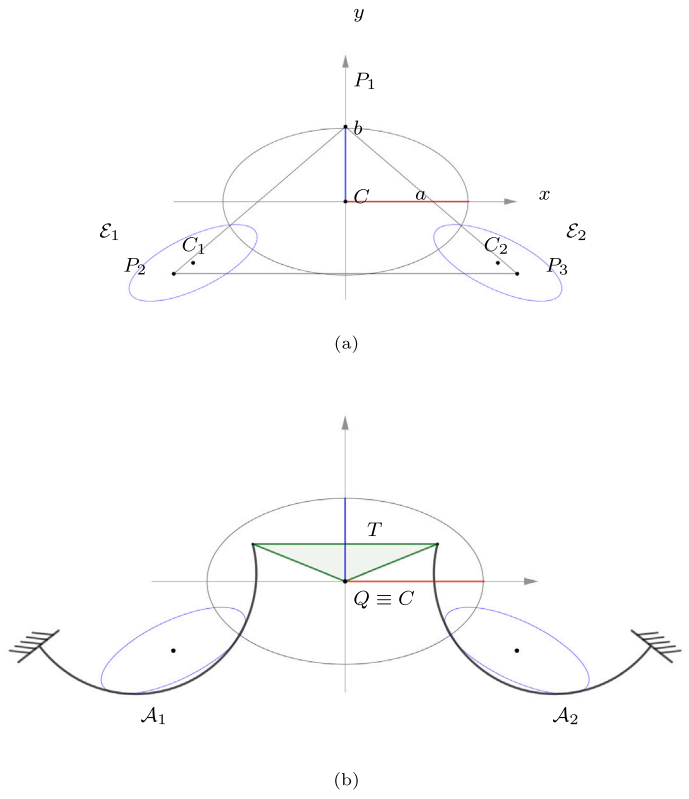

Fig. 19. Closed-chain synthesis: primary ellipse, the common self-polar triangle, and the secondary ellipses (a), and materialized compliant mechanism (b).

Table 3
Geometric and elastic parameters of the closed-chain compliant mechanism and of its corresponding ellipses of elasticity. Angles in radians, lengths in millimeters, flexural rigidities in N mm^2. The angle σ defines the orientation of the arc bisector with respect to the x-axis.

Self-polar Triangle											
P_1				P_2				P_3			
x	y	w_i/w	ν_1	x	y	w_i/w	ν_1	x	y	w_i/w	ν_1
0	15.28	0.491	0.500	−35.03	−14.73	0.255	0.021	35.03	−14.73	0.255	0.979
Secondary ellipses of elasticity											
$\mathcal{E}_1$						$\mathcal{E}_2$					
x_C	y_C	a	b	χ	w_P/w	x_C	y_C	a	b	χ	w_P/w
−31.09	−12.52	14.27	5.32	0.45	13.33	31.09	−12.52	14.27	5.32	0.45	13.33
Compliant mechanism											
$\mathcal{A}_1$						$\mathcal{A}_2$					
x_O	y_O	r	σ	γ	EI	x_O	y_O	r	σ	γ	EI
−37.88	1.56	21.85	−1.12	1.37	286.5	37.88	1.56	21.85	1.12	1.37	286.5

Considering the same load conditions of the open-chain case, the theoretical analysis is performed by applying Eq. (27). The theoretical and the numerical results are reported in Table 4. Also in this case, the numerical results confirm the theoretical predictions, with errors below 0.7%.

8. Conclusions

In this paper, a novel approach for the synthesis of planar compliant mechanisms, namely the projective synthesis method, is presented. The method is based on the antiprojective polarity properties of the ellipses of elasticity, defined in the weighted projective plane. This approach enables the extension of single-point relations to single-body relations.

The procedure consists of defining a primary ellipse of elasticity on the basis of the assigned requirements, regardless of the physical definition of the elastic suspension. Then, the ellipse is geometrically decomposed into n−ary ellipses, to satisfy the required

Table 4
Closed-chain compliant mechanism synthesis: generalized displacements obtained with the theoretical approach and with FEA simulations. Forces in Newton, lengths in millimeters, angles in radians.

Load		Theory			FEA		
Type	Magnitude	δ_x	δ_y	θ	δ_x	δ_y	θ
$\boldsymbol{f_x}$	1.0	3.53	0.00	0.000	3.52	0.00	0.000
$\boldsymbol{f_y}$	1.0	0.00	9.80	0.000	0.00	9.77	0.000
$\boldsymbol{m}$	10.0	0.00	0.00	0.157	0.00	0.00	0.156

topology. Any configuration composed of substructures in series and parallel arrangements can be obtained. The top-down procedure guarantees the positive definiteness of the kinetostatic relations at every level of the decomposition.

The lowest-level ellipses can be materialized into a variety of elastic elements, connected through several patterns of rigid links. As a result, multiple solutions to the synthesis problem can be achieved, defining compliant mechanisms that are equivalent from a linear kinetostatics point of view. This feature can be exploited to avoid mechanical interference and meet secondary or off-design issues, as motion of intermediate links, manufacturing, or footprint requirements. The projective synthesis method does not require optimization algorithms, post-processing refinements, or the definition of a rigid-body mechanism. However, it could serve as an effective framework for further optimization steps.

The method has been applied to the synthesis of two compliant mechanisms, characterized by open and closed chains. The results have been verified through finite element analyses.

CRediT authorship contribution statement

O. Sorgonà: Writing – review & editing, Writing – original draft, Validation, Software, Methodology, Formal analysis, Conceptualization. **O. Giannini:** Writing – review & editing, Validation, Formal analysis, Conceptualization. **M. Verotti:** Writing – review & editing, Writing – original draft, Validation, Supervision, Methodology, Conceptualization.

Declaration of competing interest

The authors declare that they have no known competing financial interests or personal relationships that could have appeared to influence the work reported in this paper.

Data availability

No data was used for the research described in the article.

References

[1] L. Chen, An integral approach for large deflection cantilever beams, Int. J. Non-Linear Mech. 45 (3) (2010) 301–305.
[2] M. Batista, Large deflections of shear-deformable cantilever beam subject to a tip follower force, Int. J. Mech. Sci. 75 (2013) 388–395.
[3] A. Mukherjee, S.F. Ali, A. Arockiarajan, Compliant structure under follower forces and any combined loading: Theoretical and experimental studies, Int. J. Mech. Sci. 153–154 (2019) 75–82.
[4] J. Zhu, G. Hao, Modelling of a general lumped-compliance beam for compliant mechanisms, Int. J. Mech. Sci. 263 (2024) 108779.
[5] A.A. Nobaveh, G. Radaelli, W.W. van de Sande, R.A. van Ostayen, J.L. Herder, Characterization of spatially curved beams with anisotropically adaptive stiffness using sliding torsional stiffeners, Int. J. Mech. Sci. 234 (2022) 107687.
[6] G. Hao, J. Yu, H. Li, A brief review on nonlinear modeling methods and applications of compliant mechanisms, Front. Mech. Eng. 11 (2) (2016) 119–128.
[7] M. Ling, L.L. Howell, J. Cao, G. Chen, Kinetostatic and dynamic modeling of flexure-based compliant mechanisms: A survey, Appl. Mech. Rev. 72 (3) (2020) 030802.
[8] P. Bilancia, M. Baggetta, G. Hao, G. Berselli, A variable section beams based bi-BCM formulation for the kinetostatic analysis of cross-axis flexural pivots, Int. J. Mech. Sci. 205 (2021) 106587.
[9] S. Li, G. Hao, Design and nonlinear spatial analysis of compliant anti-buckling universal joints, Int. J. Mech. Sci. 219 (2022) 107111.
[10] O. Ochoa, M. Betancourt-Tovar, A.S. Espinosa-Curiel, A. Castro-Avilés, N. Granados, E. Cuan-Urquizo, Novel compliant mechanism-based auxetic metamaterial: Kinematic and experimental analysis, Int. J. Mech. Sci. 279 (2024) 109478.
[11] J.M. McCarthy, B. Roth, Instantaneous properties of trajectories generated by planar, spherical, and spatial rigid body motions, J. Mech. Des. 104 (1) (1982) 39–50.
[12] E. Pennestri, N.P. Belfiore, On the numerical computation of generalized burmester points, Meccanica 30 (2) (1995) 147–153.
[13] B. Roth, On the advantages of instantaneous invariants and geometric kinematics, Mech. Mach. Theory 89 (2015) 5–13.
[14] O. Sorgonà, O. Giannini, M. Verotti, Single-point synthesis of compliant mechanisms, Precis. Eng. Submitted (2024).
[15] M. Verotti, High-order kinematics of uniform flexures, Mech. Mach. Theory 196 (2024) 105631.
[16] O. Sigmund, K. Maute, Topology optimization approaches: A comparative review, Struct. Multidiscip. Optim. 48 (6) (2013) 1031–1055.
[17] Y. Liu, Y. Oda, K. Sasahara, Shape and topology optimization method with generalized topological derivatives, Int. J. Mech. Sci. 284 (2024) 109735.
[18] H. Wang, W. Yu, G. Chen, An approach of topology optimization of multi-rigid-body mechanism, Comput.- Aided Des. 84 (2017) 39–55.
[19] L. Cao, A.T. Dolovich, A. Chen, W.C. Zhang, Topology optimization of efficient and strong hybrid compliant mechanisms using a mixed mesh of beams and flexure hinges with strength control, Mech. Mach. Theory 121 (2018) 213–227.
[20] B. Zhu, X. Zhang, H. Zhang, J. Liang, H. Zang, H. Li, R. Wang, Design of compliant mechanisms using continuum topology optimization: A review, Mech. Mach. Theory 143 (2020) 103622.

[21] B. Niu, X. Liu, M. Wallin, E. Wadbro, Topology optimization of compliant mechanisms considering strain variance, Struct. Multidiscip. Optim. 62 (3) (2020) 1457–1471.
[22] P. Bilancia, G. Berselli, An overview of procedures and tools for designing nonstandard beam-based compliant mechanisms, Comput.- Aided Des. 134 (2021) 103001.
[23] C. Leng, G. Hao, X. Ren, C. Wang, Y. Li, Y. Zhang, H. Li, A synthesis approach of XYZ compliant parallel mechanisms toward motion decoupling with isotropic property and simplified manufacturing, J. Mech. Des. 146 (11) (2024).
[24] Handbook of Compliant Mechanisms, Wiley, 2013, http://dx.doi.org/10.1002/9781118516485.
[25] P. Sanò, M. Verotti, P. Bosetti, N.P. Belfiore, Kinematic synthesis of a D-drive MEMS device with rigid-body replacement method, J. Mech. Des. 140 (7) (2018).
[26] L.L. Howell, A. Midha, Parametric deflection approximations for end-loaded, large-deflection beams in compliant mechanisms, J. Mech. Des. 117 (1) (1995) 156–165.
[27] H.-J. Su, A pseudorigid-body 3R model for determining large deflection of cantilever beams subject to tip loads, J. Mech. Robot. 1 (2) (2009) 021008.
[28] Y.-Q. Yu, P. Zhou, Q.-P. Xu, A new pseudo-rigid-body model of compliant mechanisms considering axial deflection of flexural beams, in: New Trends in Mechanism and Machine Science, Springer, 2015, pp. 851–858.
[29] V.K. Venkiteswaran, H.-J. Su, Pseudo-rigid-body models for circular beams under combined tip loads, Mech. Mach. Theory 106 (2016) 80–93.
[30] Y.-Q. Yu, S.-K. Zhu, 5R pseudo-rigid-body model for inflection beams in compliant mechanisms, Mech. Mach. Theory 116 (2017) 501–512.
[31] M. Verotti, A pseudo-rigid body model based on finite displacements and strain energy, Mech. Mach. Theory 149 (2020) 103811.
[32] M. Cera, M. Cirelli, L. Colaiacovo, P.P. Valentini, Second-order approximation pseudo-rigid model of circular arc flexure hinge, Mech. Mach. Theory 175 (2022) 104963.
[33] J.B. Hopkins, M.L. Culpepper, Synthesis of multi-degree of freedom, parallel flexure system concepts via freedom and constraint topology (FACT) – part I: Principles, Precis. Eng. 34 (2) (2010) 259–270.
[34] J.B. Hopkins, M.L. Culpepper, Synthesis of multi-degree of freedom, parallel flexure system concepts via freedom and constraint topology (FACT). Part II: Practice, Precis. Eng. 34 (2) (2010) 271–278.
[35] J.B. Hopkins, J. Rivera, C. Kim, G. Krishnan, Synthesis and analysis of soft parallel robots comprised of active constraints, J. Mech. Robot. 7 (1) (2015).
[36] N.C. Archer, J.B. Hopkins, Large-range rotation-to-translation compliant transmission mechanism, J. Mech. Des. 145 (12) (2023).
[37] N.C. Archer, J.B. Hopkins, Analysis and synthesis of interconnected hybrid mechanisms using freedom and constraint topologies (FACT), Mech. Mach. Theory 200 (2024) 105722.
[38] H. Li, G. Hao, A constraint and position identification (CPI) approach for the synthesis of decoupled spatial translational compliant parallel manipulators, Mech. Mach. Theory 90 (2015) 59–83.
[39] H. Li, Y. Liu, Z. Wang, C. Leng, Z. Zhang, G. Hao, A constraint-flow based method of synthesizing $XY\theta$ compliant parallel mechanisms with decoupled motion and actuation characteristics, Mech. Mach. Theory 178 (2022) 105085.
[40] C.J. Kim, S. Kota, Y.-M. Moon, An instant center approach toward the conceptual design of compliant mechanisms, J. Mech. Des. 128 (3) (2005) 542–550.
[41] C.J. Kim, Y.-M. Moon, S. Kota, A building block approach to the conceptual synthesis of compliant mechanisms utilizing compliance and stiffness ellipsoids, J. Mech. Des. 130 (2) (2008).
[42] C. Li, S.-C. Chen, Design of compliant mechanisms based on compliant building elements. part I: Principles, Precis. Eng. 81 (2023) 207–220.
[43] C.J. Kim, On the geometry of stiffness and compliance under concatenation, J. Mech. Robot. 12 (2) (2020).
[44] H. Lipkin, T. Patterson, Geometrical properties of modelled robot elasticity: Part I — decomposition, in: International Design Engineering Technical Conferences and Computers and Information in Engineering Conference, 22nd Biennial Mechanisms Conference: Robotics, Spatial Mechanisms, and Mechanical Systems, 1992, pp. 179–185, http://dx.doi.org/10.1115/DETC1992-0213.
[45] H. Lipkin, T. Patterson, Geometrical properties of modelled robot elasticity: Part II — center of elasticity, in: International Design Engineering Technical Conferences and Computers and Information in Engineering Conference, 22nd Biennial Mechanisms Conference: Robotics, Spatial Mechanisms, and Mechanical Systems, 1992, pp. 187–193, http://dx.doi.org/10.1115/DETC1992-0214.
[46] G. Krishnan, C. Kim, S. Kota, An intrinsic geometric framework for the building block synthesis of single point compliant mechanisms, J. Mech. Robot. 3 (1) (2010).
[47] O. Sorgonà, N. Belfiore, O. Giannini, M. Verotti, Application of the ellipse of elasticity theory to the functional analysis of planar compliant mechanisms, Mech. Mach. Theory 184 (2023) 105308.
[48] O. Sorgonà, S. Serafino, O. Giannini, M. Verotti, Analysis of compliant mechanisms with series and parallel substructures through the ellipse of elasticity theory, Int. J. Solids Struct. 298 (2024) 112847.
[49] J.N. Reddy, Energy Principles and Variational Methods in Applied Mechanics, third ed., John Wiley & Sons, Hoboken, New Jersey, 2017.
[50] M. Faggella, R. Gigliotti, G. Mezzacapo, E. Spacone, Graphic dynamic prediction of polarized earthquake incidence response for plan-irregular single story buildings, Bull. Earthq. Eng. 16 (10) (2018) 4971–5001.
[51] T. Hughes, J. Cottrell, Y. Bazilevs, Isogeometric analysis: CAD, finite elements, NURBS, exact geometry and mesh refinement, Comput. Methods Appl. Mech. Engrg. 194 (39–41) (2005) 4135–4195.
[52] C.V. Jutte, S. Kota, Design of single, multiple, and scaled nonlinear springs for prescribed nonlinear responses, J. Mech. Des. 132 (1) (2009).
[53] G. Radaelli, J.L. Herder, Shape optimization and sensitivity of compliant beams for prescribed load-displacement response, Mech. Sci. 7 (2) (2016) 219–232.
[54] S.F. Hosseini, B. Moetakef-Imani, S. Hadidi-Moud, B. Hassani, Pre-bent shape design of full free-form curved beams using isogeometric method and semi-analytical sensitivity analysis, Struct. Multidiscip. Optim. 58 (6) (2018) 2621–2633.
[55] B.D. Upadhyay, S.S. Sonigra, S.D. Daxini, Numerical analysis perspective in structural shape optimization: A review post 2000, Adv. Eng. Softw. 155 (2021) 102992.
[56] O. Weeger, Isogeometric sizing and shape optimization of 3D beams and lattice structures at large deformations, Struct. Multidiscip. Optim. 65 (2) (2022).